Proceedings 10th NUMGE 2023
10th European Conference on Numerical Methods in Geotechnical Engineering
Zdravkovic L, Kontoe S, Taborda DMG, Tsiampousi A (eds)

https://doi.org/10.53243/NUMGE2023-141

A nonlinear kinematic hardening model for ratcheting in clays

D. Abadias[1] , E. Ushev[2] , L. Zdravkovic[3]

[1] *Geowynd Ltd, London, UK*
[2] *ARUP, London, UK*
[3] *Department of Civil and Environmental Engineering, Imperial College London, London, UK*

ABSTRACT: This paper presents a cyclic total stress constitutive model, using a novel nonlinear kinematic hardening framework for the modelling of clays under cyclic loading. While the nonlinear kinematic hardening rules have been widely used to describe ratchetting and cyclic behaviour of rubbers and metals, they are less popular in the field of geomaterials. The new model illustrates how the nonlinear kinematic framework can be adapted to include aspects of soil behaviour such as those observed at small strains, or the Lode's angle-dependency of the yield surface in the deviatoric plane, while allowing for the control of the strain accumulation. The model's response is compared against triaxial cyclic experiments performed on a stiff, low-plasticity glacial clay till from the Bolders Bank formation, including data for 100 cycles at various load amplitudes. The comparison is very favourable, showing a strong potential of the proposed constitutive framework for the realistic modelling of cyclic loading of geomaterials.

Keywords: Ratchetting modelling, Constitutive models, Stiff Clays

1 INTRODUCTION

The modelling of ratchetting in geotechnical engineering is an area that has gained substantial interest in the context of recent developments in offshore wind. Generally, the typical cyclic loads experienced by an offshore wind sub-structure can be classified in two main groups: extreme large amplitude cases, representative of the 35-hour extreme storms, and medium to small amplitude cases typically representing the 25-year operational life of the turbine.

This presents a challenge for the application of soil constitutive models, as the cyclic nature of the load requires accurate modelling of large amplitudes in two-way conditions (storms) and of medium to small amplitudes in one-way conditions (operational), under a significantly high number of cycles. Models that address ratchetting in 1D conditions have been proposed within the framework of hyperplasticity (Houlsby, 2017), however, very few models exist in the formulation of the nonlinear kinematic framework that is more commonly used to model ratchetting in other engineering disciplines.

In order to capture the complex soil-structure interaction in the conditions of offshore wind turbines under variable environmental loads advanced constitutive models are required, capable of predicting the soil response to a wide range of amplitudes and cyclic loading conditions (one-way, two-way). This paper presents a constitutive model developed in the nonlinear kinematic framework to specifically address the ratcheting in geomaterials (Abadias, 2019). The model formulation is briefly introduced, followed by its calibration and predictions in the context of undrained triaxial monotonic and cyclic testing of a stiff, low-plasticity glacial clay till (Ushev, 2018)

2 MODEL FORMULATION

This total stress model is formulated within the framework of nonlinear kinematic hardening rules (NLKH). NLKH rules were first developed by Armstrong and Frederick (1968) and have been widely expanded in the context of metals and rubbers. The present model is applicable to ductile clays and borrows concepts from cyclic plasticity such as the backstress superposition (Chaboche, 1991) and the dynamic recovery terms (Ohno and Wang, 1993) to enhance its ratchetting capabilities. In addition, the model also combines principles of hypoplasticity (Wu and Niemunis, 1996) to include the Lode's angle dependency of the limit surface and its generalisation in the stress space.

2.1 Notation

The following definitions are included for clarity. The deviatoric component of a stress tensor is defined as

$$A_{ij}^{d} = A_{ij} - 1/3\, A_{kk}\delta_{ij} \qquad (1)$$

where δ_{ij} is the second order identity and A_{kk} is the trace of *A*. The norm of a tensor is expressed as:

$$\|A_{ij}\| = \sqrt{A_{ij}A_{ij}} \tag{2}$$

while the normalized direction of a tensor is

$$\vec{A}_{ij} = A_{ij}/\|A_{ij}\| \tag{3}$$

and the time derivative of A_{ij} is defined as

$$\dot{A}_{ij} = \frac{\partial A_{ij}}{dt} \tag{4}$$

2.2 Yield surface

Being a total stress model, it is independent of the mean stress. The model falls in the framework of the J2 plasticity and the yield surface does not have a Lode's angle dependency. For simplicity, the yield surface is formulated as a metric of the elastic region in tensorial notation as:

$$\|\sigma_{ij}^d - \sum\alpha_{ij}^d\| = m \tag{5}$$

where α_{ij}^d is the deviatoric part of each backstress history variable and σ_{ij} is the stress tensor.

2.3 Flow rule

The model is associated, hence the normal to the yield surface and the plastic flow direction coincide. In this case, as Equation (5) is expressed as a norm, the derivatives are also unitary and equal:

$$\vec{n}_{ij} = \vec{m}_{ij} = \frac{\sigma_{ij}^d - \sum\alpha_{ij}^d}{m} \tag{6}$$

where $\vec{m}_{ij}$ is the derivative of the potential function and $\vec{n}_{ij}$ the derivative of the yield surface. Hence, the plastic strain is straightforward:

$$\dot{\varepsilon_{ij}^p} = \lambda\vec{n}_{ij} \qquad \lambda = \|\dot{\varepsilon_{ij}^p}\| \tag{7}$$

2.4 Hardening rules

The response of the model under monotonic and cyclic behaviour is governed by the hardening rule. The advantage of the NLKH rules with respect to other frameworks lies in its simple yield surface and its associated flow. As a result, it is possible to embed complex characteristics of the soil behaviour through the hardening rules. Examples of extensions to the NLKH rules are detailed for more complex soils and in effective stress conditions in Abadias (2019).

For the final definition of the model the history variables are defined. The model has five backstresses, $\alpha_{ij}^{(k)}$, and the evolution of each one is described by a general hardening rule as:

$$\dot{\alpha_{ij}^{(k)}} = E_k(\dot{\varepsilon_{ij}^p} - Y^{(k)}\,\alpha_{ij}^{(k)}/\|\alpha_{ij}^{(k)}\|\,\|\dot{\varepsilon_{ij}^p}\|) \tag{8}$$

where E_k controls the intial stiffness and $Y^{(k)}$ the assimptotic response. The function $Y^{(k)}$ represents the failure envelope of the material and "k" represents the backstress number. The definition of the limit surface follows Grimstad et al. (2012) and is embedded in the asymptotic response using the same methodology, for each hardening rule, proposed in Wu and Niemunis (1996) as:

$$Y^{(k)} = \left(\frac{\sqrt{3/2\alpha_{ij}^{(k)}\alpha_{ij}^{(k)}}}{s_u^\theta}\right)^{\chi^{(k)}} \tag{9}$$

where S_u^θ includes the undrained shear strength Lode's angle dependency in the deviatoric failure plane:

$$S_u^\theta = \frac{3S_u^C}{(\sqrt{3}(1+S_u^C/S_u^E)\cos\theta - 3(1-S_u^C/S_u^E)\sin\theta)} \tag{10}$$

Finally, $\chi^{(k)}$ in equation (9) controls the rate at which the model reaches asymptotic conditions.

2.5 Monotonic and cyclic asymptotic behaviour

The proposed model is rate independent, hence time and plastic flow are linear, similar to the endochronic theory of Valanis (1978). In this sense Equation (8) can be treated as an ordinary differential equation and its response can be assessed through a phase diagram for its asymptotic properties. The asymptote of Equation (8) in monotonic conditions is:

$$Y^{(k)} = 1 \tag{11}$$

which is clearly in line with the definition of the limit surface in the hypoplasticity theory. On the other hand, under cyclic conditions, the asymptotic behaviour of each orbit is governed by the non-linear term in Equation (8). This is illustrated when integrating Equation (8) over a strain-controlled closed cycle, giving:

$$\Delta\alpha^{(k)} = E_k \int_{\|\varepsilon_{ij}^t\|}^{\|\varepsilon_{ij}^{t+1}\|} \vec{\alpha}_{ij,t+1}^d Y_{t+1}^{(k)} - \vec{\alpha}_{ij,t}^d Y_t^{(k)} \tag{12}$$

where the measure $\Delta\alpha^{(k)}$ represents the change of the backstress with respect to an unclosed cycle of amplitude $\|\varepsilon_{ij}^{t+1}\| - \|\varepsilon_{ij}^t\|$, with $\vec{\alpha}_{ij,t+1}^d$, $Y_{t+1}^{(k)}$, $\vec{\alpha}_{ij,t}^d$, $Y_t^{(k)}$ being the values at the crest (t+1) and trough (t) of the cycle.

Hence, from Equation (12) it is possible to infer the ratchetting characteristics of the model under cyclic conditions. The following characteristics are a consequence of Equation (12):

- Under two-way loading conditions the model always shakes down ($\Delta\alpha^{(k)} = 0$);
- Under strain-controlled conditions, regardless of the two way or one-way loading, there always exists a stress loop where the model shakes-down ($\Delta\alpha^{(k)} = 0$);
- Under unsymmetric stress-controlled conditions a single law produces constant ratcheting ($\Delta\alpha^{(k)} = constant$).

The implications of Equation (12) for a single NLKH rule are shown graphically in Figure 1 for 5 cycles. It can be seen that there always exists a closed orbit under strain-controlled conditions (see One-Way strain controlled + and − lines) and that the ratcheting is constant per cycle under one-way stress loading conditions (see One-Way load controlled).

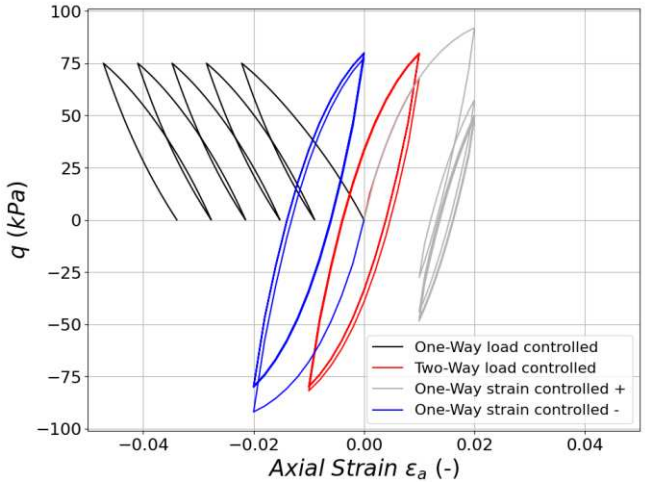

Figure 1. Illustration of stable and unstable orbits for the proposed hardening rule

2.6 Modelling of ratchetting

It is clear that the mathematical form of the NLKH model intrinsically reproduces ratchetting with a single backstress in one-way stress conditions. When several are combined, the evolution of each backstress interacts with each other allowing for non-linear ratchetting modelling (Chaboche, 1991, Ohno and Wang, 1993).

To further improve the ratchetting response the present model includes a memory backstress history variable, in addition to the five hardening rules, defined as:

$$\dot{X}_{ij} = \begin{cases} k\dot{\varepsilon}_{ij}^{p} & if\ \|X_{ij}\| < M \\ 0 & if\ \|X_{ij}\| = M \end{cases} \quad (13)$$

which alters the metric of the limit surface in Equation (9) for each hardening rule:

$$Y^{(k)} = \left(\frac{\sqrt{3/2(\alpha_{ij}^{(k)} - X_{ij})(\alpha_{ij}^{(k)} - X_{ij})}}{s_u^{\theta}} \right)^{\chi^{(k)}} \quad (14)$$

With the modification proposed in Equation (14) the model adds even more flexibility regarding the calibration of cyclic stable orbits. Thanks to the modifications proposed, a stable orbit does not require the symmetry between crest and through of the cycle to shake down. In this sense the proposed modification modifies the nature of NLKH rules where the metric of the plastic modulus depends on the current state of the backstress is more in line with bounding surface plasticity (Dafalias, 1986).

3 CALIBRATION METHODOLOGY

The calibration of the proposed constitutive model is reasonably straightforward and follows the same principles of other NLKH models under monotonic and cyclic conditions (e.g. Rezaiee-Pajand, 2009).

3.1 Monotonic conditions

The shapes of stress-strain curves can be calibrated using the superposition principle. For illustration purposes the following equations are proposed as a good approximation, in this case for the five hardening rules:

$$E_k = \begin{cases} (q_k - q_0)/(\varepsilon_k - \varepsilon_0) & k = 1 \\ \frac{q_k - q_{k-1}}{\varepsilon_k - \varepsilon_{k-1}} - \frac{q_{k+1} - q_k}{\varepsilon_{k+1} - \varepsilon_k} & k = 2,..,n = 5 \end{cases} \quad (15)$$

$$s_u^k = \begin{cases} (q_k - q_0)/2 & k = 1 \\ (q_k - q_{k-1})/2 & k = 2,..,n = 5 \end{cases} \quad (16)$$

while the $\chi^{(k)}$ can be set manually to accommodate the concavity of each hardening rule, or can be determined through a numerical optimisation procedure.

3.2 Cyclic conditions

For the model calibration under cyclic conditions, it is recommended to adjust the undrained shear strength of each backstress, S_u^k, to half the amplitude of the cyclic load that is wished to calibrate the model against.

The first backstress should be stiffer than the second and so on, which is similar to carrying out the calibration of the model in monotonic conditions. It must be noted that the best strategy is a procedure where the low amplitude cycles are captured by the first stiffer backstress NLKH rules and the large amplitudes by the softer backstresses NLKH rules.

The calibration of accumulated strain versus number of cycles of different amplitudes is resolved using Equations (12) and (13). The detailed procedure is outlined in Abadias (2019) where the response under a number

of cycles can be hindcasted from the asymptotic behaviour of Equation (12) for the sum of all NLKH rules. A wide range of calibration procedures for NLKH are possible under cyclic conditions and can be found in the literature, e.g. Rezaiee-Pajand (2009) or Bari et al, (2000).

4 APPLICATION TO COWDEN CLAY TILL LABORATORY TESTS

The performance of the proposed model is examined at a level of a single integration point, against the laboratory and field characterisation of the glacial clay at Cowden (Zdravkovic et al., 2020). The laboratory data used for the benchmarking of the model is part of a wider experimental programme carried out by Ushev (2018) and Ushev and Jardine (2022b).

4.1 Monotonic tests

The calibration methodology described above is directly applicable to the ductile monotonic stress-strain curves of the Cowden clay till. The parameter $\chi^{(k)}$ controls the curvature and evolution, allowing for accurate matching of any stress-strain curve.

Figure 2 shows an example stress-strain curve from undrained shearing in triaxial compression (TXU) of a 100 mm diameter specimen, with an anisotropic initial stress state at $p' = 67.5$ kPa and $q = -25$ kPa (Ushev, 2022a). The figure demonstrates the principle behind the model calibration, showing the contribution of each of the backstresses (five in this case) as dashed lines and following the above recommendation of the first backstress producing the stiffest response to the final being the softest. The consecutive accumulative response from each backstress is shown with dotted lines, with the final solid black line representing the modelled response which is in excellent agreement with the experimental TXU curve.

This level of agreement is representative of the remaining experiments used for model calibration. The parameters derived to represent the backbone monotonic loading are summarised in Table 1.

Table 1. Calibration for TXU

	E (kPa)	S_u (kPa)	χ
NLKH-1	28450	45	0.9
NLKH-2	20580	30	0.9
NLKH-3	750	30	0.9
NLKH-4	1240	30	0.75
NLKH-5	405	14	0.75

4.2 Cyclic triaxial tests

The model is benchmarked against a selection of undrained cyclic triaxial tests conducted on Cowden till specimens by Ushev and Jardine (2022a), who characterised the cyclic response of the till with respect to the number of cycles to failure, N, mean effective stress, p', drifts, accumulation of mean and cyclic strains and the degradation of stiffness with strain.

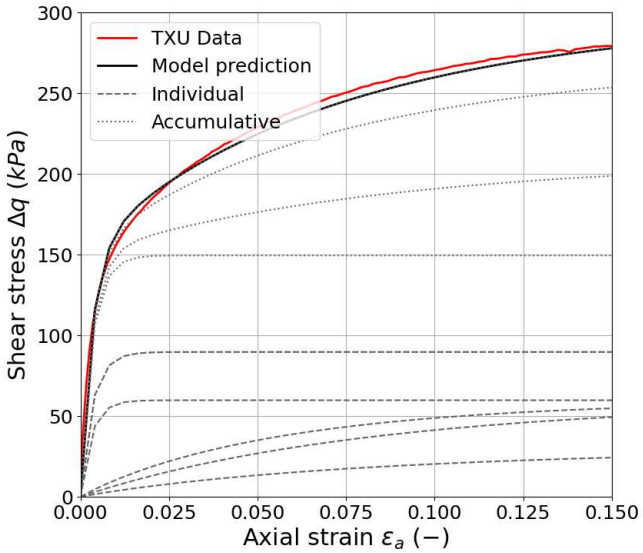

Figure 2. Bolders Bank TXU monotonic calibration

Their analysis of experimental data identified the behaviour as being highly dependent on the amplitude of cyclic loading, q_{cyc}, its mean effective stress and the relative position of the current effective stress state to the failure envelope. The response was divided into *safe* and *unsafe* zones, with two distinct failure modes in the unsafe zone, namely *abrupt* and *creeping* failures. Low cyclic amplitudes were shown to lead to decreasing strain accumulation with the number of cycles, negligible stiffness degradation and low p' drifts, allowing the till to sustain and recover its S_u. Increasing the cyclic amplitude was shown to lead to permanent strains and stiffness loss which became progressively larger as the till's effective stress paths approached the static failure line.

Table 2. Cyclic characteristics

	q_{av} (kPa)	q_{cyc} (kPa)	q_{av}/q_{cyc}
TXUCyc-1	-25.0	25.0	1.0
TXUCyc-2	-25.0	37.5	0.66
TXUCyc-3	-25.0	50.0	0.5
TXUCyc-4	-25.0	75.0	0.33

The tests selected for benchmarking the cyclic performance of the model are summarised in Table 2. They were carried out from in-situ stress states with an average deviatoric stress of $q_{av} = -25$ kPa. Their cyclic loading was also deemed representative of the typical offshore wind loading characteristics: large amplitude 2-way loading conditions and medium to low amplitude one-way operational loading conditions. The four tests selected for cyclic calibration have the deviatoric stress

amplitudes of 50, 75, 100 and 150 kPa and cyclic characteristics summarised in Table 2. The parameters q_{cyc} and q_{av} follow the cyclic load definitions of Andersen (2015).

Figure 3 shows the response of the calibrated model for each amplitude of cyclic loading. The figure demonstrates the model's ability to accommodate a wide range of ratcheting phenomena, from shakedown to linear stabilisation and energy dissipation per cycle, being dependent on the amplitude and characteristics of the load cycle. All numerical predictions shown in Figure 3 correspond to a single set of model parameters, which is essential when applying any constitutive model in analyses of boundary value problems that involve variable stress amplitudes through the modelled domain.

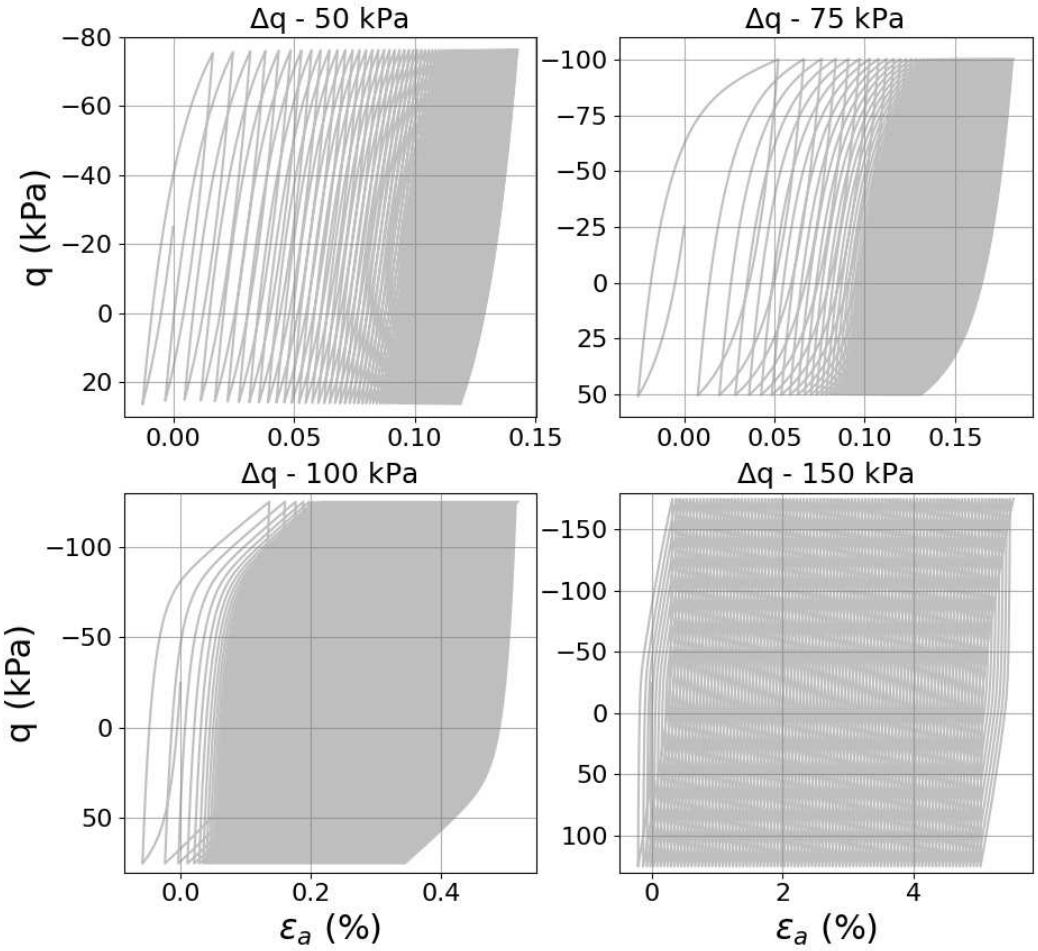

Figure 3. Model prediction for 50, 75, 100 and 150 kPa deviatoric stress amplitudes

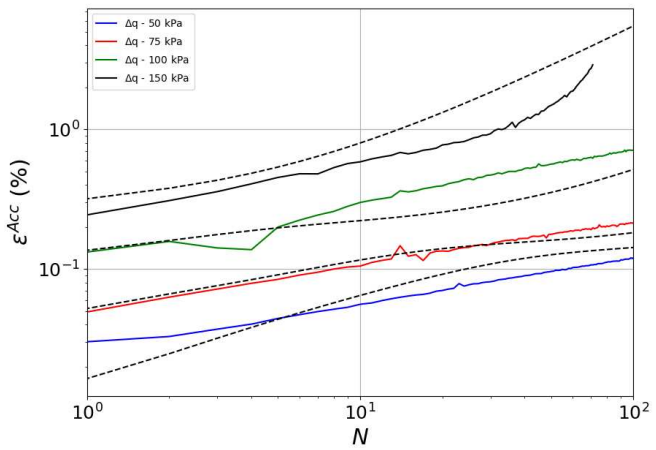

Figure 4. Model predictions(dashed lines) vs Bolders Bank experiments for $q_{av} = -25$ kPa (experimental data after Ushev and Jardine, 2022a)

A comparison of the accumulated axial strain, ε^{acc}, versus the number of cycles, N, is shown in Figure 4 for 100 cycles applied in the triaxial tests listed in Table 2. The model predictions are shown as dashed lines while the test data is shown in colours. The comparison is very favourable, further confirming the ability of the constitutive model to accurately capture the cyclic response of the clay with a single set of model parameters.

Although not shown here for brevity, the proposed model is also capable of capturing ratchetting acceleration and shakedown for varying amplitudes and unsymmetric loading conditions, allowing the reproduction of the nonlinear ratchetting behaviour with the number of cycles under a variety of loading conditions.

5 CONCLUSIONS

This paper has introduced a novel constitutive model for representing the behaviour of ductile clays, developed in the framework of nonlinear kinematic hardening, combining the backstress superposition techniques and principles of hypoplasticity.

Presented here only at the level of soil element behaviour at a single integration point, the model demonstrates strong ability for accurate representation of both the monotonic and cyclic response of the clay till under undrained triaxial loading. The latter in particular is shown to capture very favourably the strain accumulation in the clay for a range of deviatoric stress amplitudes over the applied 100 loading cycles.

REFERENCES

Abadias, G.D. 2019. *Constitutive modelling of cyclically loaded soils for application in offshore engineering*. PhD Thesis, Imperial College London.

Armstrong, P.J., Frederick C.O. 1966. *A mathematical representation of the multiaxial Bauschinger effect*. Vol. 731. Berkeley, CA: Berkeley Nuclear Laboratories.

Andersen, K.H. 2015. Cyclic soil parameters for offshore foundation design. *Frontiers in offshore geotechnics III* (pp. 6-82).

Bari, S., Tasnim, H. 2000. Anatomy of coupled constitutive models for ratcheting simulation. *International Journal of Plasticity* 16 (3-4): 381-409.

Dafalias, Y.F. 1986. Bounding surface plasticity. I: Mathematical foundation and hypoplasticity. *Journal of engineering mechanics* 112 (9): 966-987.

Grimstad, G., Andresen L., Hans P.J. 2012. NGI-ADP: Anisotropic shear strength model for clay. *International journal for numerical and analytical methods in geomechanics* 36 (4): 483-497.

Houlsby, G T.,.Abadie, C.N., Beuckelaers, W.J.A.P., Byrne, B.W. 2017. A model for nonlinear hysteretic and ratcheting behaviour. *International Journal of Solids and Structures* 120: 67-80.

Ohno, N., Wang, J-D. 1993. Kinematic hardening rules with critical state of dynamic recovery, part I: formulation and basic features for ratchetting behaviour. *International Journal of Plasticity* 9 (3): 375-390.

Chaboche, J-L. 1991. On some modifications of kinematic hardening to improve the description of ratchetting effects. *International journal of plasticity* 7 (7): 661-678.

Rezaiee-Pajand, M., Sina, S. 2009. On the calibration of the Chaboche hardening model and a modified hardening rule for uniaxial ratcheting prediction. *International Journal of Solids and Structures* 46 (16): 3009-3017.

Ushev, E. 2018. *Laboratory investigation of the mechanical properties of Cowden till under static and cyclic conditions*. PhD Thesis, Imperial College London.

Ushev, E., Jardine, R.J. 2022a. The behaviour of Bolders Bank glacial till under undrained cyclic loading. *Géotechnique* 72 (1): 1-19.

Ushev, E., Jardine, R.J. 2022b. The mechanical behaviour of Bolders Bank till. *Canadian Geotechnical Journal* 59 (12): 2163-2183.

Valanis, K.C. 1978. *Fundamental consequences of a new intrinsic time measure. Plasticity as a limit of the endochronic theory*. Iowa University, Iowa City.

Wu, W., Niemunis, A. 1996. Failure criterion, flow rule and dissipation function derived from hypoplasticity. *Mechanics of Cohesive-frictional Materials: An International Journal on Experiments, Modelling and Computation of Materials and Structures* 1 (2): 145-163.

Zdravković, L., Jardine, R.J., Taborda, D.M.G., Abadias, D., Burd, H.J., Byrne, B.W., Gavin, K.G., Houlsby, G.T., Igoe, D.J.P., Liu, T., Martin, C.M., McAdam, R., Muir Wood, A., Potts, D.M., Gretlund J.S., Ushev, E. 2020. Ground characterisation for PISA pile testing and analysis. *Géotechnique* 70 (11): 945-960.